JOURNAL OF THERMOPHYSICS AND HEAT TRANSFER
Vol. 21, No. 1, January–March 2007

Characterization/Modeling of Wire Screen Insulation for Deep-Water Pipes

Dong Kim,* Carlos Silva,† Egidio Marotta,‡ and Leroy Fletcher§
Texas A&M University, College Station, Texas 77840

DOI: 10.2514/1.25886

The amount of oil consumption has been rapidly increasing around the world; consequently, industries have expanded offshore exploration into deep-sea waters. At sea-floor depths, pipe insulation is essential to prevent blockage within the pipe due to paraffin buildup within the crude oil. To maintain a proper inner crude oil temperature, above the paraffin formation point, insulation had been used to reduce heat loss. In this study, the objective was to develop an analytical model for a newly developed wire screen insulation that contains both nonconforming and conforming interfaces within the wire screen joints and then to compare the predicted results with experimentally measured data for validation. The experimental study for this novel insulation technology consisted of a coaxial pipe fabricated from P110-4140 steel with a low-conductivity wire screen (stainless steel) as the interstitial insulation material inserted at the annulus.

Nomenclature

A = area, m^2
$A + B$ = geometric parameter related to radius of curvature, $1/\mathrm{m}$
a = semimajor diameter of ellipse, m
a_c = microcontact radius, m
b = semiminor diameter of ellipse, m
c = length between nodes, m
c_1 = correlation coefficient, dimensionless
c_2 = correlation coefficient, GPa
D = diameter, m
E = modulus of elasticity, $\mathrm{N/m^2}$
E' = effective modulus of elasticity, $\mathrm{N/m^2}$
F = applied load, N
f = combination of terms, dimensionless
H = hardness, MPa
h = thermal conductance, $\mathrm{W/m^2 \cdot K}$
I_g = gap conductance integral, dimensionless
K = complete elliptic integral of first kind, dimensionless
k = thermal conductivity, $\mathrm{W/m \cdot K}$
L = length, m
M = gas parameter, m
m = absolute asperity slope, dimensionless semimajor axis parameter
N = number of microcontacts, dimensionless
n = number density of contact spot $1/\mathrm{m}^2$ semiminor axis parameter
P = pressure, $\mathrm{N/m^2}$, Pa
R = thermal resistance, $\mathrm{K/W}$
T = temperature, K
Y = mean plane separation, m
α = ratio of semimajor axes, dimensionless
Δ = physical parameter, $\mathrm{m/N}$
δ = normal deformation of surface, m
ε = relative contact spot size, dimensionless
κ = parameter, dimensionless
λ = relative mean plane separation, dimensionless
ν = Poisson's ratio, dimensionless
ρ = minimum radius of curvature, m
ρ' = maximum radius of curvature, m
σ = effective surface roughness, m
ψ = constriction parameter, dimensionless

Subscripts

a = apparent
c = constriction, contact
e = elliptic, elastic
g = gas
iw = inner wall
mc = microcontact
ow = outer wall
p = plastic
r = real
tmc = total microcontact
tot = total
w = wire of screen mesh
1–2 = surfaces 1 and 2

I. Introduction

THE high demand for oil has come from an exponential increase in transportation's use of the internal combustion engine within developed and developing countries. To meet this high demand, oil industries have explored offshore locations for more oil products. But within the deep-sea environment, temperatures can range from 0 to 2°C (32 to 35°F); thus, pipe insulation is obligatory to prevent blockage in the pipe due paraffin and hydrate buildup. Usually, crude oil contains a type of wax that begins to form solid paraffin deposits on the inner surface of the pipe when the oil temperature reaches the paraffin cloud point (68°C or 155°F); therefore, blockage can and does occur. When paraffin waxes block the inside of the pipe, an additional process is needed to remove it, which translates to reduced production efficiency. Crude oil production temperatures are typically above 70°C (159°F) and, to maintain the inner temperature above the paraffin formation point, minimization of heat loss from the pipe wall must be realized. Several insulation techniques have been developed to overcome the thermal issue by the addition of low-conductivity materials and coatings on the external pipe surface.

Presented as Paper 3135 at the 9th AIAA/ASME Joint Thermophysics and Heat Transfer Conference, San Francisco California, 5–8 June 2006; received 14 June 2006; revision received 23 August 2006; accepted for publication 24 August 2006.

*Research Assistant, Mechanical Engineering, Mail Stop 3123. Student Member AIAA.

†Research Assistant, Mechanical Engineering, Mail Stop 3123.

‡Associate Research Professor, Mechanical Engineering, Mail Stop 3123. Associate Fellow Member AIAA.

§Thomas A. Dietz Professor, Mechanical Engineering, Mail Stop 3123. Honorary Fellow Member AIAA.

However, these techniques have had severe limitations, such as damage due to large hydrostatic pressure differentials and installation concerns [1–3]. With insertion of a wire screen as an interstitial material within the annulus of a coaxial pipe, a reduction in the heat transfer rate (and, thus, retardation in paraffin buildup) can be achieved without the limitations previously stated. Moreover, the manufacture and installation process for subsea piping will be greatly simplified [4]. Within the interstitially insulated coaxial pipe, the interstitial fluid is air that remains stagnant with conduction heat transfer dominating. This is due to the fact that the air space between the coaxial pipes is small enough to prevent natural convection from occurring within the space. The dominating heat transfer mechanism of this system is conduction through nonconforming contacts between the wall and wire screen. In addition, conforming microcontacts within the screen wire and pipe wall itself provide an additional resistance heat flow path between contacting interfaces. Both macrocontact and microcontact models were reviewed and employed to develop a proper joint resistance model. To aid in the model development, a thermal network circuit was drawn to help visualize the heat path and aid in the joint model development.

A review of the literature on thermal contact resistance shows extensive publications for both experimental and analytical studies. There exist numerous papers that detail correlations and analytical models for contact resistance for rough, conforming surfaces and nonconforming contacting surfaces. These studies take various approaches; however, little work has been performed for a joint that contains both contacts simultaneously, such as a wire screen [5].

An initial analytical study by Cividino et al. [6] analyzed joint conductances for a woven wire screen using only Hertzian theory [7] to predict the macrocontact area when the wire screen contacts a solid surface. The contacting surfaces follow Hertzian theory for deformation. The authors neglected bulk resistance of wire-to-wire contacts and microresistances. However, to obtain more accurate predictions, microcontact analysis under the formed macrocontact area is required as well. This investigation develops an analytical model that combines both macro- and microcontact theory to predict the overall joint resistance for contacting surfaces containing a wire screen.

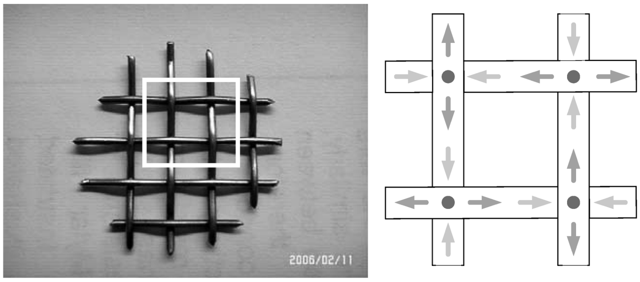

a) b)

Fig. 1 Top view of a unit cell of the screen wire and a schematic of the heat flow in a unit cell.

Lambert and Fletcher [8] reviewed contact resistance models for various cases under vacuum condition and Sridhar and Yovanovich [9] reviewed elastic and plastic models that showed that smooth, contacting surfaces deform elastically and rough surfaces deform plastically. Also, Savija et al. [10] contained an excellent review for thermal conductance models with interstitial substances inserted at the joint.

In this study, an analytical model is developed for an interstitially insulated coaxial pipe that includes both macro- and microcontact resistances and fluid gap resistances. Predictions from the model are compared with experimental data from a previous experimental study [4] (see Appendix A). The interstitial material is a low-conductivity wire screen inserted in the annulus of the coaxial pipe.

II. Thermal Circuit Modeling

Cividino et al. [6] developed an analytical model for a woven wire screen contacting a solid wall, but in this study, the bulk resistance through the screen wire and the microcontact resistances within the wires were neglected. Moreover, to have a more accurate model, the contact points among wire screen materials must also be accounted for. In the present experimental study, the actual specimen diameter was 1 in. (2.54 cm).

To properly build the thermal circuit, the nominal area must be specified and then divided into a unit cell area. Each unit cell area has four nodes. Figures 1a and 1b are the top view of the actual wire screen and a schematic, respectively. The heat flow path from the inner pipe wall to the outer pipe wall can be simplified, as shown in Figs. 2a and 2b.

For a given unit cell, four nodes are placed in parallel connection, and each node has both serial and parallel paths (resistances) [11]. The overall thermal resistance for the unit cell be written as a parallel circuit of the thermal resistances of each node, as shown in Fig. 3.

III. Contact Resistance Model

The joint analytical model was based on a combination of macrocontact resistance, microcontact resistance, microgap resistance, bulk resistance, and air resistance of a node in a unit cell and then programmed with the use of MATLAB software.

A. Macrocontact Model

Nonconforming contact modeling was the first step toward developing the model and was based on expressions in macrocontact resistance developed by Yovanovich [12]. To obtain the contact area formed by the applied load on each nodal contact, geometrical parameters for screen wire and walls [13], as shown in Fig. 2b, were calculated with the following expressions:

$$\alpha = c/D_w \tag{1}$$

$$\rho = D_w/2 \tag{2}$$

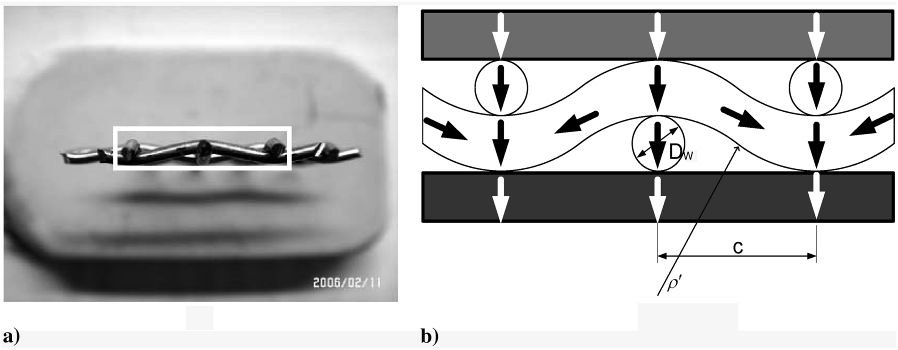

a) b)

Fig. 2 Side view of a unit cell of the screen wire and a schematic of the heat flow path.

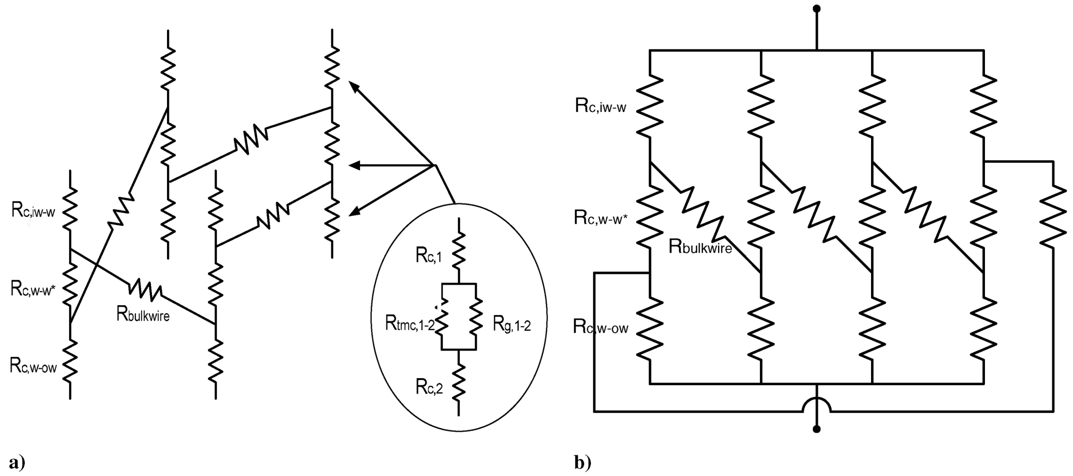

Fig. 3 Thermal circuit in a unit cell and thermal circuit in a unit cell in a closed form.

$$\rho' = (D_w/4)(1+\alpha^2) \tag{3}$$

where $\rho'$and ρ are the maximum and minimum of the radius of curvature (for flat surfaces, $\rho' = \rho = \infty$) and D_w is the wire screen diameter.

The inner and outer walls were assumed to be flat surfaces and so their curvatures were considered to be infinite. Each contact point forms an elliptical contact area with semimajor and semiminor axes a and b computed as follows:

$$a = m\left[\tfrac{3}{4}F\Delta\right]^{\frac{1}{3}}, \qquad b = n\left[\tfrac{3}{4}F\Delta\right]^{\frac{1}{3}} \tag{4}$$

where m and n are obtained from the following expressions [13] for the range of values $2 < \alpha < 8$, and F and Δ are shown next.

$$m = 0.830\alpha^{0.735}, \qquad m/n = 0.7905\alpha^{1.18} \tag{5}$$

$$F = PA_{\text{apparent}} = Pc^2 \tag{6}$$

$$\Delta_{1-2} = \frac{\left\{\left[\left(1-\nu_1^2\right)/E_1\right] + \left[\left(1-\nu_2^2\right)/E_2\right]\right\}}{A+B} \tag{7}$$

$$A + B = \frac{1}{2}\left[\frac{1}{\rho_1} + \frac{1}{\rho_1'} + \frac{1}{\rho_2} + \frac{1}{\rho_2'}\right] \tag{8}$$

Because the formed elliptical contact area is very small when compared with the nodal area, the thermal resistance in the contact area can be modeled as a thermal constriction-spreading resistance within half-space (Yovanovich [12]). With calculated semimajor and semiminor axes, the thermal constriction resistance for the contact area of each node can be determined as

$$R_{\text{constriction}} = \psi_e^T/4ka \tag{9}$$

where ψ_e^T is the spreading/constriction parameter defined as [13]

$$\psi_e^T = \tfrac{2}{\pi}K(\kappa) \tag{10}$$

with κ defined as

$$\kappa = [1 - (b/a)^2]^{1/2} \tag{11}$$

The constriction-spreading resistance between the two different materials is the summation of each constriction resistance:

$$R_{\text{constriction}12} = R_{c1} + R_{c2} \tag{12}$$

A total of three constriction-spreading resistances exist for each nodal contact (e.g., $R_{\text{iw}-w}$, R_{w-w}, and $R_{w-\text{ow}}$).

B. Bulk Resistance (Wire)

In the thermal circuit, some portion of the heat flow within the wire between each node must be taken into account, as shown in Fig. 3. Analyzing the circuit network via Kirchhoff's current law [14], the amount of heat outflow and inflow must be constant and can be modeled as a parallel resistance with the wire-to-wire constriction resistance and bulk resistance. The bulk resistance through the wire was defined as

$$R_{\text{bulkwire}} = 2L/k_w A_w \tag{13}$$

where A_w (defined next) is the wire cross-sectional area

$$A_w = \pi D_w^2/4, \qquad L = \sqrt{c^2 + D_w^2} \tag{14}$$

C. Microcontact Resistance

Within the elliptical contact area formed by the applied load, a number of conforming microcontacts are also formed; therefore, microconstriction/spreading and gap resistances coexist in parallel. Generally, each surface has roughness for which all contacting asperity was assumed to be isotropic and randomly distributed over the contacting surfaces (i.e., Gaussian surface [15]).

Between two Gaussian surfaces, the contact can be simplified as a flat/rough surface with an effective roughness and slope. The effective rms surface roughness and effective absolute mean asperity slope were computed as

$$\sigma = \sqrt{\sigma_1^2 + \sigma_2^2}, \qquad m = \sqrt{m_1^2 + m_2^2} \tag{15}$$

Depending on the deformation mode of the contacting asperities, two model types are available: plastic or elastic. With geometric parameters obtained from each model, the contact resistances can be obtained with the use of the following relationships [16]. Details of these models are further explained in the following sections.

$$h_c = 2nak_s/\psi(\varepsilon) \tag{16}$$

$$k_s = \frac{2k_1k_2}{k_1 + k_2} \tag{17}$$

$$\psi(\varepsilon) = (1-\varepsilon)^{1.5}, \qquad \varepsilon = \sqrt{A_r/A_a} \tag{18}$$

D. Plastic Model

If contacting asperities are deformed plastically, then the following relationships via Cooper et al. [16] and Yovanovich [17] are applicable with appropriate geometric parameters:

$$\lambda = (Y/\sigma)_p = \sqrt{2}erfc^{-1}(2P/H_p) \tag{19}$$

$$a_c = \sqrt{\frac{8}{\pi}\frac{\sigma}{m}}\exp\left(\frac{\lambda^2}{2}\right)erfc\left(\frac{\lambda}{\sqrt{2}}\right) \tag{20}$$

$$n = \frac{1}{16}\left(\frac{m}{\sigma}\right)^2 \frac{\exp(-\lambda^2)}{erfc(\lambda/\sqrt{2})} \tag{21}$$

$$\frac{A_r}{A_a} = \frac{1}{2}erfc\left(\frac{\lambda}{\sqrt{2}}\right) \tag{22}$$

where A_r/A_a is the ratio of actual contact area to nominal area. In Eq. (19), H_p is the microhardness of the softer contacting asperities.

An appropriate microhardness can be obtained from the relative contact pressure P/H_P relationship developed by Song et al. [18]:

$$\frac{P}{H_p} = \left[\frac{P}{c_1(1.62\sigma/m)^{c_2}}\right]^{1/(1+0.071c_2)} \tag{23}$$

where c_1 and c_2 are obtained from Vickers microhardness measurements. Equivalent Vickers microhardness can be computed from Brinell hardness values H_B:

$$\begin{aligned} &c_1/3178 = 4.0 - 5.77H_B^* + 4.0(H_B^*)^2 - 0.61(H_B^*)^3 \\ &H_B^* = H_B/3178 \qquad c_2 = -0.370 + 0.442(H_B/c_1) \end{aligned} \tag{24}$$

E. Elastic Model

The elastic deformation model for contacting asperities was initially proposed by Mikic [19] as follows:

$$\lambda = (Y/\sigma)_e = \sqrt{2}erfc^{-1}(4P/H_e) \tag{25}$$

$$a_c = \frac{2}{\sqrt{\pi}}\frac{\sigma}{m}\exp\left(\frac{\lambda^2}{2}\right)erfc\left(\frac{\lambda}{\sqrt{2}}\right) \tag{26}$$

$$n = \frac{1}{16}\left(\frac{m}{\sigma}\right)^2 \frac{\exp(-\lambda^2)}{erfc(\lambda/\sqrt{2})} \tag{27}$$

$$\frac{A_r}{A_a} = \frac{1}{4}erfc\left(\frac{\lambda}{\sqrt{2}}\right) \tag{28}$$

$$H_e = CmE', \qquad C = 0.7071 \tag{29}$$

$$\frac{1}{E'} = \frac{1-\nu_1^2}{E_1} + \frac{1-\nu_2^2}{E_2} \tag{30}$$

where H_e and $1/E'$ are the equivalent elastic hardness and the effective Young's modulus, respectively.

With appropriate geometrical parameters and either the plastic or elastic model, the microcontact thermal resistance can be computed as

$$R_{\mathrm{mc}} = 1/h_c\pi a_c^2 \tag{31}$$

For a given nodal area, the total microcontact resistance was calculated with the following expression:

$$R_{\mathrm{tmc}} = R_{\mathrm{mc}}/N_{\mathrm{mc}} \tag{32}$$

where $N_{\mathrm{mc}} = n \times A_e$, $A_e = \pi ab$, and N_{mc} is within the nodal area A_{node}.

F. Microgap Resistance

In the present investigation, the space within the wall and wire screen and the microgap between the contacting interfaces was filled with air, which is the media of conduction across the gap. The gap conductance model was first developed by Yovanovich [17] as

$$h_g = (k_g/\sigma)I_g \tag{33}$$

A correlation equation for the gap integral I_g was developed by Negus and Yovanovich [20], which depends on two dimensionless parameters: the relative mean planes separation Y/σ and the relative gas rarefaction parameter M/σ.

$$I_g = \frac{f_g}{(Y/\sigma) + (M/\sigma)} \tag{34}$$

where

$$f_g = 1.063 + 0.0471(4 - \tfrac{Y}{\sigma})^{1.68}(\ell n\, \tfrac{\sigma}{M})^{0.84}$$

The gas's dependence on pressure and temperature for the gas parameter M was presented by Yovanovich et al. [21] as

$$M = 0.373 \times 10^{-6} \times \frac{T_{\mathrm{air}}}{323} \times \frac{P_{g,1\mathrm{atm}}}{P_g} \tag{35}$$

With these parameters, the microgap resistance for a node was obtained as

$$R_g = 1/h_g\pi ab \tag{36}$$

G. Air Resistance in the Space Within Wall and Wire Screen

The interstitial area between the inner and outer wall was occupied with air and wire screen, and the area not occupied by the wire screen is the cross-sectional area occupied by trapped air. The area of the unit cell is $A_{\mathrm{node}} = c^2$. Thus, the occupied air cross-sectional area was computed as

$$A_{\mathrm{air}} = A_{\mathrm{node}} - (2 \times c \times D_w - D_w^2) \tag{37}$$

When the load was applied to the node, each contact point was deformed in the same direction as the applied load for which deformation can be obtained from the expression developed by Johnson [7]:

$$\delta = \frac{3F}{2\pi abE'}bK(\kappa) \tag{38}$$

Therefore, the thermal resistance through the air in the space for each deformed node and air space can be expressed as (this expression takes into account the wire deformation and its influence on the distance of the air space)

$$R_{\mathrm{air}} = \frac{2D_w - \delta_{\mathrm{iw}-w} - \delta_{w-w} - \delta_{w-\mathrm{ow}}}{k_{\mathrm{air}}A_{\mathrm{air}}} \tag{39}$$

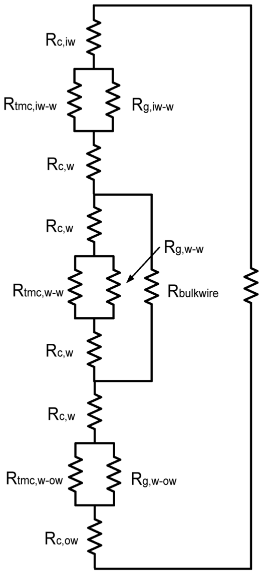

Fig. 4 Total thermal circuit for a node.

H. Total Resistance

The total contact resistance for each node from the inner wall to the wire mesh and then to the outer wall is a summation of all the resistances that are in serial and parallel, as shown in Fig. 4.

The following expressions detail the equations used to calculate each component. For the inner or outer wall and wire screen, the following expressions were used:

$$R_{c,\mathrm{iw}-w} = R_{c,\mathrm{iw}} + \left(\frac{1}{R_{\mathrm{tmc,iw}-w}} + \frac{1}{R_{g,\mathrm{iw}-w}}\right)^{-1} + R_{c,w} \tag{40}$$

$$R_{c,w-\mathrm{ow}} = R_{c,w} + \left(\frac{1}{R_{\mathrm{tmc},w-\mathrm{ow}}} + \frac{1}{R_{g,w-\mathrm{ow}}}\right)^{-1} + R_{c,\mathrm{ow}} \tag{41}$$

For the resistance of the wire screen, the following expression was employed:

$$R_{c,w-w} = \left(\frac{1}{(R_{c,w} + \{[1/(R_{\mathrm{tmc},w-w})] + [1/(R_{g,w-w})]\}^{-1} + R_{c,w})} + \frac{1}{R_{\mathrm{bulkwire}}}\right)^{-1} \tag{42}$$

The total contact resistance of each node was calculated from the summation of the contact points, as follows:

$$R_{\mathrm{tot},c} = R_{c,\mathrm{iw}-w} + R_{c,w-w} + R_{c,w-\mathrm{ow}} \tag{43}$$

The total contact resistance was in parallel with the air space resistance shown in Fig. 4 and computed as

$$R_{\mathrm{tot,node}} = \left(\frac{1}{R_{\mathrm{tot},c}} + \frac{1}{R_{\mathrm{air}}}\right)^{-1} \tag{44}$$

One unit cell has four nodes that exist as parallel resistances; therefore, the total resistance for the unit cell becomes

$$R_{\mathrm{tot,cell}} = \left(\frac{4}{R_{\mathrm{tot,node}}}\right)^{-1} \tag{45}$$

The number of unit cells in an actual area can obtained from the following expression:

$$N_{\mathrm{cell}} = \frac{A_{\mathrm{actual}}}{A_{\mathrm{cell}}} \tag{46}$$

In a similar manner, actual joint thermal resistance and conductance can be expressed as

$$R_{\mathrm{actual}} = \left(\frac{N_{\mathrm{cell}}}{R_{\mathrm{tot,cell}}}\right)^{-1} \tag{47}$$

$$h_{\mathrm{actual}} = \frac{1}{R_{\mathrm{actual}} A_{\mathrm{actual}}} \tag{48}$$

IV. Result and Discussion

In the present study, both macro- and microplastic and elastic models were employed. The developed model includes constriction/spreading resistances for an elliptical contact area, the bulk resistance for the wire screen, and an air space resistance for a contacting node. Plastic and elastic models for microcontacts and gap-resistance models were employed.

To investigate the contribution of each resistance to the overall resistance in a node, total contact resistance and air resistance and the total resistance for a node are plotted as a function of applied pressure, as shown in Fig. 5. This figure indicates that the contact resistance decreases as applied pressure increases, but the air resistance decreases only slightly. The contact resistance was sharply deceased due to increasing contact area. When the applied pressure reached roughly 283 kPa, the contact resistance crosses the air resistance and, thereafter, the air resistance dominates the total resistance.

The contact resistances within a node can be classified into either contact resistance by the inner-wall-to-wire, wire-to-wire, or wire-to-outer-wall resistance. In the model, the inner-wall-to-wire and wire-to-outer-wall resistances have similar properties; therefore, they are similar resistance components. Figure 6 shows a plot of the total contact resistance and contact resistances for the inner-wall-to-wire and wire-to-wire resistances. As shown in the figure, the inner-wall-to-wire or wire-to-outer-wall contact creates higher resistance than the wire-to-wire contact resistance (thus, controlling the overall resistance for the range of applied pressures investigated). The resistance in the wire-to-wire contact has a relatively large decrease as 200 kPa is approached, as indicated by the changing slope of the curve.

To obtain a better understanding of the contact resistance caused by the wall-to-wire interface, which seems to dominate the overall resistance in the node, a plot of multiple interface resistances is shown in Fig. 7. From Fig. 7, the dominant resistance component at the inner-wall-to-wire interface is clearly the microcontact resistance (R_{tmc} indicates total microcontact) that is highly dependent on the applied interface pressure. The analysis also indicates that the macroconstriction ($R_{c,\mathrm{iw}}$) and spreading ($R_{c,w}$) resistances at the inner wall and wire are the least dominant resistances, and then this is followed by the microgap resistance ($R_{g,\mathrm{iw}-w}$). All of these resistances are located at the inner-wall-to-wire interface.

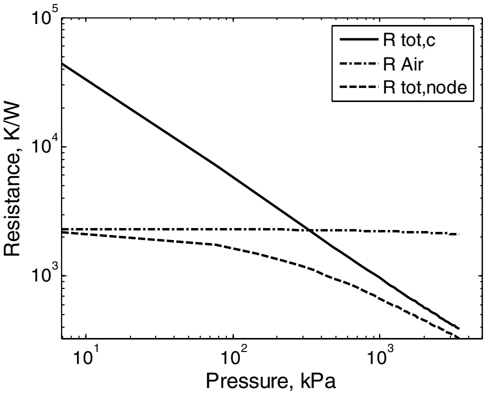

Fig. 5 Thermal resistance as a function of applied pressure in a node.

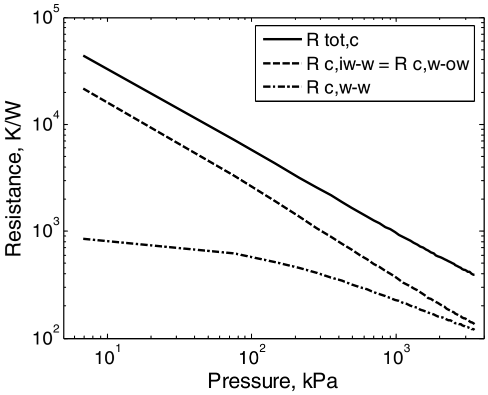

Fig. 6 Contact thermal resistance as a function of applied pressure in a node.

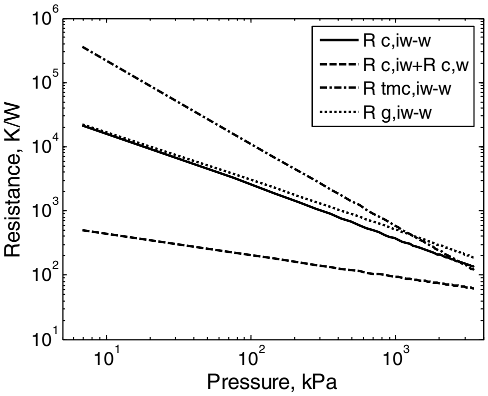

Fig. 7 Each thermal resistance as a function of applied pressure within the inner wall and wire of a node.

To highlight the same behavior within the wire-to-wire interface, Fig. 8 shows the same individual contact and gap resistances at this interface. Even in wire-to-wire contact, the total microcontact resistance ($R_{\mathrm{tmc},w-w}$) seems to be the dominant resistance parameter, similar to the inner-wall-to-wire interface shown in Fig. 7. Again, the least influence at this interface comes from the macroconstriction and spreading resistances.

However, the addition of the bulk wire resistance does cause a lower overall total contact resistance when compared with the inner-wall-to-wire interface, which is indicated by the solid lines ($R_{c,\mathrm{iw}-w}$ and $R_{c,w-w}$) in both Figs. 7 and 8. This lower resistance is more prevalent between 230 and 600 kPa of applied pressure. The overall total contact resistance includes all of the resistances that comprise the thermal circuit network (see Fig. 4 for a single node).

V. Comparison Between Model and Experiment Data

To investigate the effects of contact resistance as a function of applied pressure at a node, a nondimensionalized expression was developed that includes macrocontact, microcontact, microgap, bulk wire, and the air resistance in the space between the inner and outer wall and within the screen mesh, $R_{\mathrm{tot},c}/R_{\mathrm{tot,node}}$:

$$\frac{R_{\mathrm{tot},c}}{R_{\mathrm{tot,node}}} = 1 + \frac{R_{\mathrm{tot},c}}{R_{\mathrm{air}}} \tag{49}$$

Equation (49) is plotted in Fig. 9 as a function of applied nominal pressure over the range 1 kPa $\leq P \leq$ 3500 kPa. It seems, from this analysis, that the interface contact resistances have a greater influence on the overall resistance over all pressure regions. Further, contact resistances are sharply decreased as the applied pressure approaches 283 kPa, which is mainly caused by the reduction in microcontact resistance.

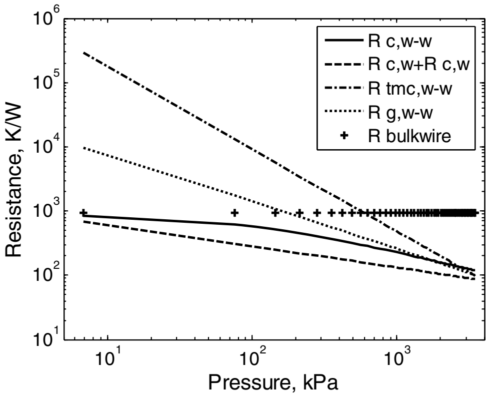

Fig. 8 Each thermal resistance as a function of applied pressure within the wire and wire of a node.

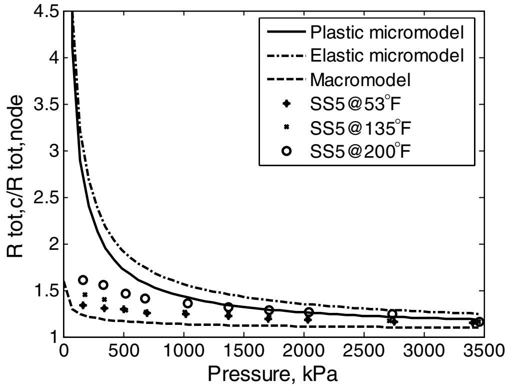

Fig. 9 Dimensionless thermal resistance as a function of applied pressure.

For comparison, experimental data are shown along with the model predictions. The trend indicates a large reduction in contact resistance influence as the pressure is increased up to 690 kPa, then the air resistance begins to dominate for pressures greater than 1015 kPa. The comparison indicates that the inclusion of a plastic model for microcontacts was better at predicting the experimental data than the assumption of elastic microcontacts at these higher pressures (rms errors have been computed). As shown by Figs. 7 and 8, the resistance due to microcontacts and microgaps is much larger than other resistances and thus becomes the controlling factor for this system. This means that a wire screen can be a proper insulating medium for an interstitially insulated system if the applied pressure is controlled properly.

The total thermal resistance for three different deformation models is compared against experimental data, as shown in Fig. 10. The comparison indicates that the trends for the total thermal resistance variation (which include the effects for plastic and elastic deformation) are similar, but that the elastic model shows a higher resistance. The difference between the two contact models is mainly caused by the deformation mode of the contacting asperities in microcontact, and generally rough surfaces tend to follow the plastic model rather than the elastic deformation model. However, the elastic macromodel by itself has lower resistance and tends to underpredict the experimental thermal resistance results.

Figure 11 plots the thermal conductance for the various models employed in this study against the experimental data. In this plot, a significant underprediction at light pressure range is observed (for micromodels, especially) for applied pressures under 1500 kPa. This is a similar trend to that shown in Fig. 10 for light applied pressures.

As a quantitative comparison between model predictions and experimental data, Table 1 shows the rms error between these results. For the plastic contact model, the error ranged from 10 to 19%, which happens to be the lowest values. With the assumption of elastic microcontact deformation, the rms error ranged from 19 to 29%.

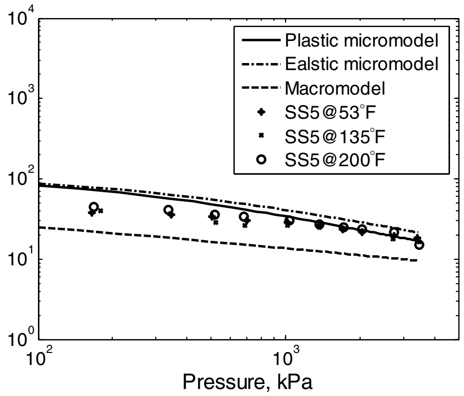

Fig. 10 Thermal resistance of each model and experimental data as a function of applied pressure.

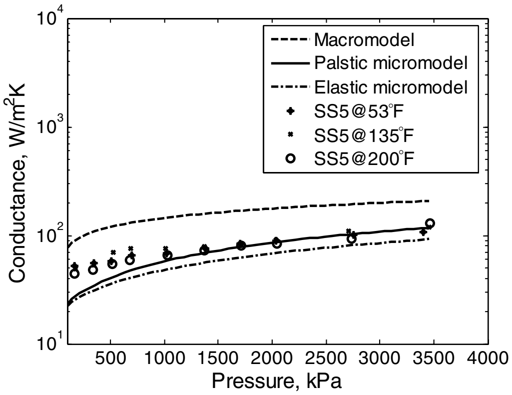

Fig. 11 Thermal conductance of each model and experimental data as a function of applied pressure.

Although these values are higher than for the plastic deformation assumption, they are still lower than for the assumption of just macrocontact without inclusion of microcontact effects. In the macromodel (does not include microcontact effects), the error ranged from 68 to 78%, which is due to the assumption of perfect contact in the deformed area.

Table 2 shows the geometrical and thermophysical properties of the metallic materials that were used for this analytical and experimental study.

In summary, the reason for higher conductance/lower resistance at lighter pressures (light applied load) compared with the model predictions can be accounted for from visual inspection of the wire screen before any testing. In the untested state, predeformation was observable at each wire-to-wire interface for each node caused by the stresses of the fabrication process. The applied load due to fabrication formed an initial contact area that results in lower resistance and higher conductance when compared with the model predictions. The model predictions do not take into account predeformation of any contacting surfaces.

Table 1 RMS error between the experimental data and models

Model	53°F	135°F	200°F	Average
Elastic Micro	29	29	19	26
Plastic Micro	19	19	10	16
Macro	68	69	78	72

VI. Conclusions

Macro- and microcontact resistance models were used to predict the performance of an interstitially insulated coaxial pipe system that contained a wire screen. The model developed shows good agreement with experimentally measured conductance values over an applicable pressure range. The intended interface pressure on the wire screen mesh will be approximately 14.7 psia (101.3 kPa) for this technology. At this interface pressure, the model underpredicts the experimentally measured conductance; however, this may be due to predeformation of the contacting wires. This leads to the discrepancy between the model and the experimental data at light interface pressures. This can be avoided if the manufacturing process is well controlled.

The wire screen acted as the interstitial insulation, which dramatically increased the thermal resistance when compared with a bare pipe. Therefore, the rate of heat loss from the inner hot wall to the outer cold wall was dramatically decreased by two orders of magnitude, as indicated by the drop in thermal conductance from roughly 2500 to 50 $\mathrm{W/m^2K}$. In addition, this study modeled the influences of several contact models that included macrocontacts and microcontacts at the interfaces of contacting surfaces.

For modeling purposes, the properties of P110-4140 pipe were used for the inner and outer wall material, and stainless steel 316 for the screen wire properties was employed for the interstitial insulation material. From modeling results, the predicted thermal conductance ranged from 44.7 to 207 $\mathrm{W/m^2K}$ for just the macrocontact model, from 17 to 118 $\mathrm{W/m^2K}$ with inclusion of the plastic model, and from 17 to 93 $\mathrm{W/m^2K}$ for the elastic model. The experimentally measured thermal conductance values ranged from 52 to 108 $\mathrm{W/m^2K}$ at an interstitial mean temperature of 53°F case, from 49 to 119 $\mathrm{W/m^2K}$ for the 135°F case, and from 44 to 129 $\mathrm{W/m^2K}$ for the 200°F case.

The average rms errors were calculated for the various model predictions and compared with the experimentally measured values. Incorporating only the macrocontact model gave an upper value of 72%, whereas the inclusion of a plastic deformation model for microcontacts gave an upper value of 16%. The assumption of elastic microcontact deformation at the interfaces gave an upper value of 26%. Clearly, among the three deformation models, the inclusion of plastic microcontacts with elastic macrocontact deformation shows good results throughout the entire pressure range, with especially excellent agreement at higher pressures.

However, at lighter pressures, further study is needed to account for the overprediction, but one possible reason for this discrepancy was observed. Predeformation of the contact area within the wire-to-wire interface was clearly witnessed that can be attributed to wire tension forces from the fabrication process.

Microcontact resistances by the wire screen were found to be the dominant resistance parameter from modeling analysis results. Therefore, by modifying the geometrical, mechanical and thermophysical properties of the wire screen, one can control the performance of the interstitially insulated coaxial pipe system. The developed model will be used to optimize the design for the actual product by varying the aforementioned parameter. The analytical modeling for this interstitially insulated system was validated against experimentally measured data with very good agreement at higher pressure.

Table 2 Properties of materials

Material	Poisson's ratio	Modulus, GPa	Roughness, μm	Absolute asperity slope	Thermal conductivity, W/mK
Steel 4140 P110 (inner or outer wall)	0.3	207	1.5	0.0938	42.7 ~ 46.7
Stainless steel 316 (mesh screen)	0.3	190	0.4	0.0471	16.3 ~ 16.5
C (length between nodes, mm)		25.4	D_w (wire diameter, mm)		0.925

Appendix A: Experiment Apparatus Overview

The thermal contact conductance (TCC) system [4] consists of a heat source, three specimens (flux meter, steel 4140 cylinder, and wire mesh), a heat sink, a load cell, and bellows. The apparatus is intended to handle specimens 1 in. in diameter. Steel 4140 bar stock was machined into 1-in-diam cylinders. The purpose of the inserts was to simulate the inner and outer piping of the interstitial insulating coaxial pipe. One cylinder insert would be in contact with the heated flux meter and the other would be in contact with the cooled flux meter. The wire mesh was sandwiched between the two cylinder inserts, thus mimicking the actual interstitially insulated coaxial pipe technology under actual temperature and pressure conditions of a subsea environment.

The bell jar's contents can be entirely evacuated if needed, thus minimizing convection heat transfer at the contact interface and all other surfaces (thus minimizing convective losses); however, these experiments were run with an ambient environment within the bell jar and, therefore, air was present between the gap formed by the contacting surface/wire screen joint.

The gap between the surfaces minimizes the convective heat transfer, but allows for conductive heat transfer to occur; therefore, the present assembly takes advantage of the low thermal conductivity of air.

The heater was attached to the upper plate and affixed to the heat source at the top of the column. The heat sink was fastened at the bottom of the column and fed with coolant. The refrigerated bath, with a temperature range of −20°C (−4°F) to 150°C (302°F), was controlled by a thermoregulator. To optimize heat transfer, coolant was used on all contacting surfaces that experienced heat flow. Radiation shields were placed around the test column to minimize radial heat loss. The shield was located approximately 2.54 cm (1 in.) from the heat source surface and 1.27 cm (0.5 in.) from the specimen.

The test column was loaded by introducing pressure into the stainless steel bellows, mounted at the bottom of the column, using a pressure regulator. A 22,241 N (5000 lbf) load cell was used to determine the pressure at the interface. Five T-type thermocouples were affixed to the centerline of each flux meter by packing them tightly into holes, using powdered metal. The test column may be operated in a vacuum environment to eliminate the effects of interstitial fluids on the heat transfer at the interface. The roughing pump works in series with an oil diffusion pump to maintain the vacuum at a low level. An uncertainty analysis was performed for each applied pressure that indicated a percent uncertainty error that ranged from 6.75 to 8.15%.

Acknowledgments

We would like to thank the Offshore Technology Research Center (Texas A&M University) and the Minerals Management Service (MMS) for their support of this project 509-35663.

References

[1] Anon., "Sub-Sea Insulation," *World Pipelines*, May 2004: pp. 49–54.

[2] Choqueuse, Dominique, Angele Chomard, and Christian Bucherie, "Insulation Materials for Ultra Deep Sea Flow Assurance: Evaluation of the Material Properties," Offshore Technology Research Center, Rept. OTC14115, 2002: pp. 1–8.

[3] Hallot, Raymond, Angele Chomard, and Stephane Couprie, "I1s: A Passive Insulation Solution to Answer Cool Down Time Challenges on Deep Water Flowlines," Offshore Technology Research Center, Rept. OTC14117, 2002: pp. 1–10.

[4] Marotta, E. E., and Fletcher, L. S., "Interstitially Insulated Coaxial Pipe," Minerals Management Service and Dept. of Mechanical Engineering, Offshore Technology Research Center, Rept. CHTL-05-509-35663, 2005: pp. 2–3, 24–25.

[5] Yovanovich, M. M., and Marotta, E. E., *Thermal Spreading and Contact Resistances, Heat Transfer Handbook*, Wiley, New York, 2003, Chap. 4.

[6] Cividino, S., Yovanovich, M. M., and Fletcher, L. S., "A Model for Predicting the Joint Conductance of a Woven Wire Screen Contacting Two Solids," *AIAA/ASME Thermophysics and Heat Transfer Conference*, AIAA, New York, 1974, pp. 1–17; also AIAA Paper 74-695.

[7] Johnson, K. L., *Contact Mechanics*, Cambridge Univ. Press, Cambridge, England, U.K., 1985.

[8] Lambert, M. A., and Fletcher, L. S., "Review of Models for Thermal Contact Conductance of Metals," *Journal of Thermophysics and Heat Transfer*, Vol. 11, No. 2, 1997, pp. 129–140.

[9] Sridhar, M. R., and Yovanovich, M. M., "Review of Elastic and Plastic Contact Conductance Models: Comparison with Experiment," *Journal of Thermophysics and Heat Transfer*, Vol. 8, No. 4, 1994, pp. 633–640.

[10] Savija, I., Culham, J. R., Yovanovich, M. M., and Marotta, E. E., "Review of Thermal Conductance Models for Joints Incorporating Enhancement Materials," *Journal of Thermophysics and Heat Transfer*, Vol. 17, No. 1, 2003, pp. 43–52.

[11] Mills, A. F., *Heat Transfer*, 2nd ed., Prentice–Hall, Upper Saddle River, NJ, 1999.

[12] Yovanovich, M. M., "Thermal Constriction Resistance Between Contacting Metallic Paraboloids: Application to Instrument Bearings," *AIAA Thermophysics Conference*, AIAA, New York, 1970, pp. 337–358; also AIAA Paper 70-857.

[13] Cividino, S., "Thermal Constriction Resistance of Woven Screen Between Parallel Plates in a Vacuum," Dept. of Mechanical Engineering, Univ. of Waterloo Rept. ME 751, Waterloo, Ontario, Canada, Dec. 1972.

[14] Rizzoni, G., *Principles and Applications of Electrical Engineering*, Irwin, Scarborough, Ontario, Canada, 1993.

[15] Francis, H. A., "Application of Spherical Indentation Mechanics to Reversible and Irreversible Contact Between Rough Surfaces," *Wear*, Vol. 45, No. 2, 1975, pp. 221–269.

[16] Cooper, M. G., Mikic, B. B., and Yovanovich, M. M., "Thermal Contact Conductance," *International Journal of Heat and Mass Transfer*, Vol. 17, 1974, pp. 205–214.

[17] Yovanovich, M. M., "Thermal Contact Correlations," *Spacecraft Radiative Transfer and Temperature Control*, edited by T. E. Horton, Vol. 83, Progress in Astronautics and Aeronautics, AIAA, New York, 1982, pp. 83–95.

[18] Song, S., Yovanovich, M. M., and Nho, K., "Thermal Gap Conductance: Effects of Gas Pressure and Mechanical Load," *Journal of Thermophysics and Heat Transfer*, Vol. 6, No. 1, 1992, pp. 62–68.

[19] Mikic, B. B., "Thermal Contact Conductance: Theoretical Considerations," *International Journal of Heat and Mass Transfer*, Vol. 12, 1969, pp. 279–300.

[20] Negus, K. J., and Yovanovich, M. M., "Correlation of Gap Conductance Integral for Conforming Rough Surfaces," *Journal of Thermophysics and Heat Transfer*, Vol. 12, 1988, pp. 279–281.

[21] Yovanovich, M. M., Culham, J. R., and Teertstra, P., "Calculating Interface Resistance," *Electronics Cooling*, Vol. 3, No. 2, May 1997, pp. 1–7.